Inviscid, Nonadiabatic Flow About Blunt Bodies

K. H. WILSON* AND H. HOSHIZAKI†
Lockheed Missiles and Space Company, Palo Alto, Calif.

A solution is obtained to the inviscid, nonadiabatic flow field that results when energy loss by radiation becomes significant. The approach taken is to include the radiation term in the energy equation and solve the resulting conservation equations for the flow past a blunt body using an integral method. No restriction is placed on the magnitude of the radiation term. The shock-layer gas is assumed to be optically thin. This reduces the radiation term to a local energy-loss term, independent of the state of the gas in other portions of the shock layer. This assumption is valid for the majority of practical re-entry conditions. Numerical results were obtained for the flow about a sphere at freestream velocities between 30,000–60,000 fps and an altitude of 200,000 ft. The solutions show the radiation loss to have a strong effect on the shock-layer enthalpy profiles and the shock standoff distance. The reduction in the radiative heat flux at the stagnation point from the adiabatic value is shown to be a strong function of the radiation loss parameter Γ. When $\Gamma = 0.5$, the stagnation-point radiative flux is reduced by 50%.

Nomenclature

a = velocity profile coefficients
b = enthalpy profile coefficients
B = blackbody intensity, $\sigma T^4/\pi$
E = blackbody emissive power, πB
f = velocity function
g = enthalpy function
h = static enthalpy
I = radiative intensity
I_0 = conservation of mass integral
I_1 = conservation of x-momentum integral
I_2 = conservation of energy integral
j = source function
L = characteristic length (R_b for sphere)
p = static pressure
q_r = radiative energy flux
r = radius measured from body centerline
R_b = body radius
s = distance measured along direction of a ray
t = dummy variable in intensity integration
T = temperature
u = velocity component parallel to body
u_∞ = freestream velocity
v = velocity component normal to surface
x, y = body-oriented coordinate system
α = mass absorption coefficient
Γ = radiation loss parameter
δ = shock-layer thickness
$\tilde{\delta}$ = transformed shock-layer thickness
ξ = difference between body and shock angle
η = Dorodnitzyn variable
θ = body angle
K = body curvature
$\tilde{K}$ = $1 + Ky$
μ = absorption coefficient
ν = parameter characterizing planar or axisymmetric geometry
ρ = density
ρ_0 = density at standard conditions, 1.29×10^{-3} g/cm^3
σ = Stefan-Boltzmann constant
τ = optical depth
ϕ = shock angle
ω = solid angle

Subscripts

0 = stagnation point
p = Planck mean
w = wall quantities
δ = quantities immediately behind shock
∞ = freestream condition
ω = quantities taken along a specified solid angle

Presented at the AIAA Aerospace Sciences Meeting, New York, January 20–22, 1964; revision received September 3, 1964.

* Research Scientist, Research Laboratory. Member AIAA.
† Staff Scientist, Research Laboratory. Member AIAA.

1. Introduction

ENTRY velocities and trajectories of interest for planetary missions produce conditions that result in large rates of thermal radiation from the shock layer about a blunt-nosed body. For such re-entry conditions, the gas in the shock layer loses a significant fraction of its total energy by thermal radiation, and the flow may no longer be treated as adiabatic. In this paper, the nonadiabatic character of the flow is investigated by analyzing the coupled radiation and gasdynamic processes occurring in the shock layer. The flow field about axisymmetric and two-dimensional bodies is determined for cases where the shock layer is assumed to be inviscid and in complete thermodynamic equilibrium but where energy transfer by radiation is comparable to convected energy transport. The effect of nonequilibrium thermodynamic process may be significant for some of the flight conditions investigated. However, it is reasonable to consider only equilibrium flows initially leaving the nonequilibrium problem as a logical future extension of the analysis. The analysis is restricted to shock layers that are sufficiently optically thin so that self-absorption of radiation is negligible.

Early work on radiating shock layers considered problems where it was possible to uncouple the gasdynamic and radiation processes. Goulard[1] considered the stagnation-region flow for cases where the energy lost by thermal radiation is a small fraction of the total energy in the flow. Similarly, Bird[2] and Kennet[3] considered radiating flows around blunt bodies where the flow field is given essentially by an adiabatic solution. In a more recent report, Yoshikawa and Chapman[4] considered flows where a significant fraction of the total energy is lost by thermal radiation and, in addition, considered cases where self-absorption is important. However, their analysis is restricted to one-dimensional flows. It will be demonstrated later that the two-dimensional nature of the flow about blunt bodies yields temperature profiles through the shock layer which are fundamentally different from those predicted by a one-dimensional treat-

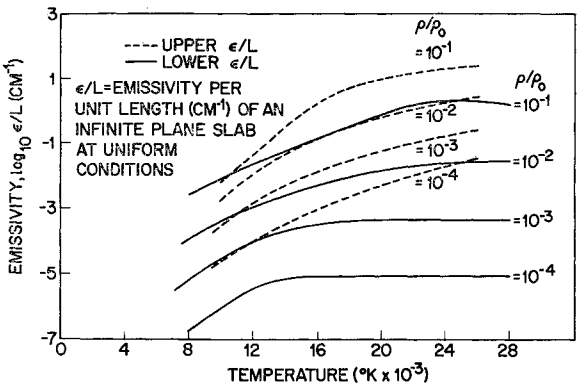

Fig. 1 Upper and lower estimate of high-temperature air emissivity.

ment. Finally, Howe,[5] who has analyzed fully coupled radiation-viscous gasdynamic flows, restricts his analysis to the region of the stagnation point of a blunt-nosed body and assumes local similarity to exist. The shock layer is assumed to be completely viscous. Numerical solutions to the appropriate conservation equations yield both the radiative and convective heating rates with full coupling taken into account.

2. Discussion of the Problem

2.1 Inviscid Flow Field

The approach taken in the present analysis is to consider the direct inviscid blunt-body problem (i.e., where the body shape is specified). The primary objective is to determine the over-all flow-field characteristics (shock shape, surface pressure distribution, etc.) and the radiative heating distribution about the body. Accordingly, an integral method is used which follows the basic approach of Maslen and Moeckel.[6] The energy equation, however, is modified to include the radiative transport term. The analysis is simplified by retaining only terms of $O(\epsilon)$ or lower (ϵ is the density ratio across the shock) in combining the governing conservation equations. The neglect of the higher-order terms in ϵ has profound effects on the ease of integrating the total differential equations that result from an integral formulation. A unique feature of the method is the manner in which the shock shape is determined. The method used is an iterative scheme in which the shock shape at each iteration is completely specified in terms of data generated from the previous iteration. An initial guess at the shock shape is obtained by assuming the shock wave to be concentric to the body. The shock shape, together with additional boundary conditions, is sufficient to determine the flow field and a new shock shape. The method yields a shock shape that converges in about three iterations to within 1% of the previously calculated

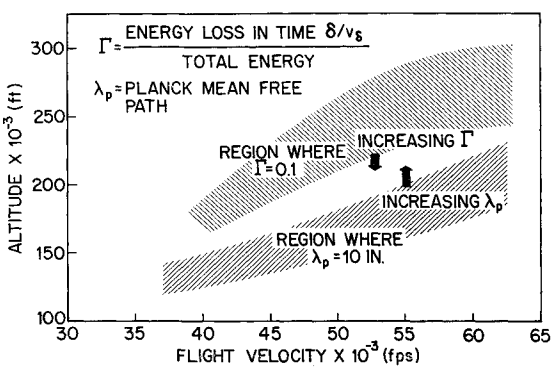

Fig 2 Flight regimes.

values. Hence, in the final analysis, no a priori information about the shock is required.

2.2 Radiative Transport Term

Before dealing with the radiative transport term, it is appropriate to discuss the radiative properties of air. At present, there is considerable disagreement between various investigators on the theoretical predictions of the emissivity of air in the important temperature region above about 12,000°K. Early work by Meyerott[7] resulted in the data shown by the solid curves in Fig. 1. This early work neglected the contributions from atomic line transitions. Recent calculations by Armstrong[8] have shown that the line transitions dominate the emissivity at about 24,000°K, and the calculations of Steward and Pyatt[9] indicate that atomic lines are significant contributors for temperatures at least as low as 18,000°K. In addition, Breene[10] has calculated the continuum contribution to the emissivity including photoionization in the wavelength region from 0.05 to 0.20 μ. Breene shows a significant contribution to the emissivity from this spectral region. In view of the lack of experimental verification of either the early or recent theoretical predictions, an upper-bound estimate (shown as dashed curves in Fig. 1) has been generated using the maximum reported emissivity in various temperature regions. Hence, Fig. 1 presents both lower and upper estimates of the emissivity of high-temperature air. Both sets of emissivity data are used in investigating the radiant energy loss from the shock layer.

The conditions under which the radiant energy loss from the shock layer is significant will be determined for both the upper and lower estimate of the emissivity of air. The radiant energy loss is important if the amount of energy lost by a fluid particle in time t, after crossing the bow shock, is a significant fraction of the initial total energy of the particle. That is, we consider the ratio

$$\Gamma = \frac{\int_0^t \nabla \cdot q_r dt}{\rho_\delta u_\infty^2/2}$$

where $\nabla \cdot q_r$ is the net local radiant energy loss rate (emission-absorption). For negligible self-absorption in the shock layer, a cold wall, a constant particle velocity, and a constant emission rate behind the bow shock, the foregoing relation can be written as

$$\Gamma = \frac{4\mu\pi B[T_\delta]\cdot\delta}{\rho_\infty u_\infty^3/2}$$

Clearly, when Γ is of $O(1)$, the flow must be considered to be nonadiabatic. In fact, nonadiabatic effects should become significant when $\Gamma = O(\frac{1}{10})$. The velocity and altitude region where $\Gamma = 0.10$ for a shock-layer thickness of 1 in. is presented in Fig. 2. The shaded region reflects the differences in the radiative properties of air as given in Fig. 1. An examination of Fig. 2 indicates that significant nonadiabatic effects can be present for flight velocities and altitudes of practical interest, using either set of emissivity data.

In Fig. 2, we also present the Planck mean free path λ_p for air behind a normal shock at the indicated velocities and altitudes, using the data of Fig. 1. It is clearly seen from Fig. 2 that, for most conditions where the radiation energy loss from a 1-in. shock layer is significant, $\lambda_p \geq 10$ in. This means that the optical depth τ of the shock layer

$$\tau = \int_0^\delta \frac{1}{\lambda_p} dy \qquad (1)$$

(or, assuming constant shock-layer properties, $\tau_\delta = \delta/\lambda_p$) is much less than unity, $\tau_\delta \ll 1$. For adiabatic flows, this

condition is sufficient to neglect self-absorption‡ (the optically thin approximation). We consider next the radiant energy loss term for nonadiabatic flows.

The physics of radiative transfer is well developed by astrophysicists (see, for example, Refs. 11–13), and Kourganoff[14] is an excellent reference on the mathematical treatment of the equation of radiative transfer in plane-parallel atmospheres. Two summaries of the equations of radiative transfer and their application to gasdynamic problems are found in Refs. 15 and 16.

Analysis of the radiative transfer equation for the case of an isothermal shock layer shows that, in the optically thin limit ($\tau_\delta \ll 1$) and assuming a cold wall, $B[T_w] \ll B[T_\delta]$, the radiative flux divergence term is

$$\nabla \cdot q_r = 4\pi\mu B[T_\delta] \tag{2}$$

where B is the blackbody intensity, and T_w and T_δ are the wall and isothermal shock-layer temperatures, respectively. Equation (2) is the familiar expression for the radiation energy loss for the case of an isothermal shock layer. It is valid when τ_δ is sufficiently small that the self-absorption term is negligible and, in addition, when the wall is very cold.

For the nonadiabatic flow under consideration, the validity of Eq. (2) must be critically examined. With radiation energy transfer, the shock layer is no longer isothermal. In fact, it is shown in the Appendix that, if we use Eq. (2), the gas temperature goes to zero at the stagnation point. Then, the local blackbody function used to determine the radiative intensity cannot be considered constant. This means that, in regions of the shock layer where the gas is relatively cool (and hence the local blackbody function relatively small), the absorption term in the flux divergence expression contains contributions from hot portions of the shock layer. Hence, it is no longer possible to judge the importance of the absorption term on the basis of the optical depth parameter τ_δ alone. As an upper bound on the importance of the contribution to the radiative intensity from the hot portions of the shock layer, we calculate the absorption term using the maximum blackbody emission in the shock layer, $B[T_\delta]$. Under this condition, again neglecting the wall emission $B[T_w]$,

$$\nabla \cdot q_r = 4\pi\mu B[T_{\text{local}}] - 2\pi\mu B[T_\delta]\tau_\delta$$

where the second term $2\pi\mu B[T_\delta]\ \tau_\delta$ is the absorption term. We now see that it is no longer adequate to have $\tau_\delta \ll 1$ in order to neglect the second term but, rather, we require§

$$B[T_\delta]\tau_\delta \ll B[T_{\text{local}}] \quad \text{or} \quad \tau_\delta \ll \frac{B[T_{\text{local}}]}{B[T_\delta]} \tag{3}$$

However, since the gas temperature (and hence $B[T]$) approaches zero at the wall when we use Eq. (2), there will always be some portion of the shock layer in which Eq. (3) is not satisfied, and at that point Eq. (2) should be modified.

Fortunately, the solutions for the temperature profile show that in only a small portion of the shock layer is the temperature low enough to cause the missing terms in Eq. (2) to be important. This means that, although the temperature as well as the enthalpy very close to the wall is not valid, the basic structure of the flow field is correct. In particular, the small region of inaccuracy in the temperature does not significantly affect the over-all conservation of mass, momentum, and energy across the shock layer, which is the basis of the integral method of solution.

‡ The need for evaluating Eq. (1) spectrally and demonstrating that $\tau_\nu \ll 1$ for all frequencies ν of interest is recognized. This requirement is particularly significant if atomic lines dominate the absorption coefficient. In view of the tenuous state of air-emissivity predictions, however, it is felt that an examination of the spectral behavior of the radiation transport term is presently not feasible.

§ The authors are indebted to P. D. Thomas of the Lockheed Missiles and Space Company Research Laboratories for pointing out that this additional restriction is necessary in order for Eq. (2) to be valid.

3. Method of Solution

3.1 Conservation Equations

The governing equations are formulated in terms of the body-oriented, boundary-layer coordinate system depicted in Fig. 3. Following Ref. 6, we normalize all variables by the following choice of nondimensional quantities:

$$\left.\begin{aligned} u &= \bar{u}/\bar{u}_\infty & v &= \bar{v}/\epsilon\bar{u}_\infty \\ x &= \bar{x}/\bar{L} & y &= \bar{y}/\epsilon L \\ \rho &= \bar{\rho}/\bar{\rho}_{\delta,0} & p &= \bar{p}/\bar{\rho}_\infty\bar{u}_\infty{}^2 \\ H &= \bar{H}/(\bar{u}_\infty{}^2/2) & h &= h/(\bar{u}_\infty{}^2/2) \\ K &= \bar{K}\bar{L} & \delta &= \bar{\delta}/\epsilon\bar{L} \\ r &= \bar{r}/\bar{L} & \alpha &= \bar{\alpha}/\alpha_{\text{ref}} \\ & & T &= \bar{T}/T_{\text{ref}} \end{aligned}\right\} \tag{4}$$

In terms of these nondimensional quantities, the conservation equations are the following:

Mass

$$(\partial r^\nu \rho u/\partial x) + (\partial \tilde{K} r^\nu \rho v/\partial y) = 0 \tag{5}$$

x Momentum

$$\rho u(\partial u/\partial x) + \tilde{K}\rho v(\partial v/\partial y) + \epsilon K\rho uv - \epsilon(\partial p/\partial x) = 0 \tag{6}$$

y Momentum

$$\epsilon\rho u(\partial v/\partial x) + \epsilon\tilde{K}\rho v(\partial v/\partial y) - K\rho u^2 + K(\partial p/\partial y) = 0 \tag{7}$$

Energy

$$\rho u(\partial H/\partial x) + \tilde{K}\rho v(\partial H/\partial y) + \beta_0\tilde{K}\rho\alpha T^4 = 0 \tag{8}$$

where

$$\tilde{K} = 1 + \epsilon K y \tag{9}$$

In the energy equation, we have introduced the mass absorption coefficient

$$\alpha = \mu/\rho \tag{10}$$

and the nondimensional energy ratio

$$\beta_0 = 8\bar{L}\bar{\alpha}_{\text{ref}}\bar{\sigma}T^4{}_{\text{ref}}/u_\infty{}^3 \tag{11}$$

For further convenience, we express Eq. (5) as

$$\frac{\partial(r/r_w)^\nu \rho u}{\partial x} + \frac{\partial \tilde{K}(r/r_w)^\nu \rho v}{\partial y} + \nu\left(\frac{r}{r_w}\right)^\nu \frac{\rho_u}{r_w}\frac{dr_w}{dx} = 0 \tag{12}$$

3.2 Integrated Form of the Conservation Equations

It has been demonstrated in Ref. 6 that the adiabatic blunt-body flow field can be calculated by integrating the mass, x-momentum, and energy equations across the shock layer and solving the resulting total differential equations. In terms of the optically thin formulation of the energy equation, the integral method carries over to the nonadiabatic case in a straightforward manner.

One can show quite generally that integrating the mass conservation equation [Eq. (5)] and applying the v-velocity boundary condition at the shock in terms of the known shock angle is completely equivalent to satisfying an over-all mass balance. That is, we equate the incoming mass flux to that passing through the shock layer of any station x and obtain the relation

$$r_\delta{}^{\nu+1} = (\nu + 1)\int_0^\delta \rho u r\, dy$$

or, upon dividing by $\rho_\delta u_\delta r_\delta^\nu$, we have

$$\frac{1}{\nu+1}\left(\frac{r_\delta}{r_w}\right)^{\nu+1}\left(\frac{r_\delta}{u_\delta}\right)=I_0 \tag{13}$$

where

$$I_0=\int_0^\delta\left(\frac{r}{r_w}\right)^\nu\frac{\rho}{\rho_\delta}\left(\frac{u}{u_\delta}\right)dy \tag{14}$$

The effects of shock-layer density variations can be reduced significantly by introducing the Dorodnitsyn variable defined by

$$\eta=\frac{\int_0^y\left(\frac{r}{r_w}\right)^\nu\left(\frac{\rho}{\rho_\delta}\right)dy}{\int_0^\delta\left(\frac{r}{r_w}\right)^\nu\left(\frac{\rho}{\rho_\delta}\right)dy}=\frac{\int_0^y\left(\frac{r}{r_w}\right)^\nu\left(\frac{\rho}{\rho_\delta}\right)dy}{\tilde\delta} \tag{15}$$

where $\tilde\delta(x)$ is the transformed shock-layer thickness. In terms of the variable η, Eq. (13) remains unchanged, and Eq. (14) becomes

$$I_0=\tilde\delta\int_0^1\left(\frac{u}{u_\delta}\right)d\eta \tag{16}$$

The x-momentum equation can be put into a form suitable for integrating across the shock layer by rewriting Eq. (6) with the aid of Eq. (12). The pressure gradient $\partial p/\partial x$ is obtained in terms of the gradient at the shock and the pressure derivative in the y direction. That is, we write

$$\frac{\partial p}{\partial x}=\frac{\partial[y(\partial p/\partial x)]}{\partial y}-y\frac{\partial^2 p}{\partial x\partial y}$$

where the last term on the right is obtained by differentiating the y-momentum equation. From Eq. (6), it is seen that the pressure gradient term is itself of $O(\epsilon)$, which means that only terms of $O(1)$ need be retained in Eq. (7) to have the analysis valid to $O(\epsilon)$. The result of these manipulations is

$$\frac{\partial(r/r_w)^\nu\rho u^2}{\partial x}+\frac{\partial K^2(r/r_w)\rho^\nu uw}{\partial y}+\left(\frac{r}{r_w}\right)^\nu\rho u^2\left[\nu\tilde K\frac{d(\ln r_w)}{dx}-\epsilon y\frac{dK}{dx}\right]+\epsilon\frac{\partial}{\partial y}\left[y\frac{\partial p}{\partial x}\right]=0 \tag{17}$$

Equation (17) can be readily integrated across the shock layer to yield, using the η variable,

$$\frac{dI_1}{dx}+\frac{2I_1}{u_\delta}\frac{du_\delta}{dx}-\left(\frac{r_\delta}{r_w}\right)^\nu\frac{d\delta}{dx}-\frac{\epsilon dK}{dx}\tilde\delta\int_0^1\left(\frac{u}{u_\delta}\right)^2\times\left[\int_0^\eta\left(\frac{\rho_\delta}{\rho}\right)d\eta'\right]d\eta+\tilde K_\delta^{\,2}\left(\frac{r_\delta}{r_w}\right)^\nu\frac{v_\delta}{u_\delta}+\frac{\nu}{r_w}\frac{dr_w}{dx}\int_0^1\tilde K\left(\frac{u}{u_\delta}\right)^2d\eta+\epsilon\delta\left(\frac{\partial p}{\partial x}\right)_\delta=0 \tag{18}$$

where

$$I_1=\tilde\delta\int_0^1\left(\frac{u}{u_\delta}\right)^2d\eta \tag{19}$$

Similarly, the energy equation can be put into a form suitable for integration across the shock layer by rewriting Eq. (8) with the aid of Eq. (12), resulting in

$$\frac{\partial}{\partial x}\left[\left(\frac{r}{r_w}\right)^\nu\rho uH\right]+\frac{\partial}{\partial y}\left[\left(\frac{r}{r_w}\right)^\nu\tilde K\rho vH\right]+\nu\times\left(\frac{r}{r_w}\right)^\nu\frac{\rho uH}{r_w}\frac{dr_w}{dx}+\left(\frac{r}{r_w}\right)^\nu\tilde K\beta_0\rho\alpha T^4=0 \tag{20}$$

which, upon integration and introduction of the η variable, yields

$$\frac{dI_2}{dx}+I_2\left[\frac{1}{u_\delta}\frac{du_\delta}{dx}+\frac{\nu}{r_w}\frac{dr_w}{dx}\right]-\left(\frac{r_\delta}{r_w}\right)^\nu\frac{d\delta}{dx}+\left(\frac{r_\delta}{r_w}\right)^\nu\tilde K_\delta\frac{v_\delta}{u_\delta}+\beta_0\tilde\delta\int_0^1\tilde K\alpha_p T^4\,d\eta \tag{21}$$

where

$$I_2=\tilde\delta\int_0^1\left(\frac{u}{u_\delta}\right)\left(\frac{H}{H_\delta}\right)d\eta \tag{22}$$

It will be noted that, contrary to the usual procedure used in boundary-layer analysis, the term v_δ is retained rather than eliminated through use of the integrated continuity equation. This approach is simply more convenient because of the availability of v_δ through the shock boundary conditions.

3.3 Boundary Conditions

The oblique shock relations provide the velocity components and pressure immediately behind the shock:

$$u_\delta=\sin\phi+\xi\cos\phi \tag{23}$$

$$v_\delta=-\cos\phi+(\xi/\epsilon)\sin\phi \tag{24}$$

$$p_\delta=(1-\epsilon)\cos^2\phi+O(\epsilon^2) \tag{25}$$

where, according to the geometry of Fig. 3,

$$\xi=\theta-\phi=\tan^{-1}\left[\frac{\epsilon}{(1+\epsilon K\delta)}\frac{d\delta}{dx}\right]$$

$$\xi=\epsilon(d\delta/dx)+O(\epsilon^2) \tag{26}$$

An additional boundary condition can be obtained by evaluating the energy equation (8) immediately behind the shock. Since the total enthalpy immediately behind the shock is a constant, Eq. (8) reduces to

$$\left.\frac{\cos\phi}{\cos\xi}\frac{\partial H}{\partial y}\right|_{\substack{x\\ y=\delta}}=-\beta_0\alpha T^4$$

From Eq. (15), the y and η variables are related by

$$\tilde\delta\,d\eta=(r_\delta/r_w)^\nu dy \qquad \text{at} \qquad y=\delta$$

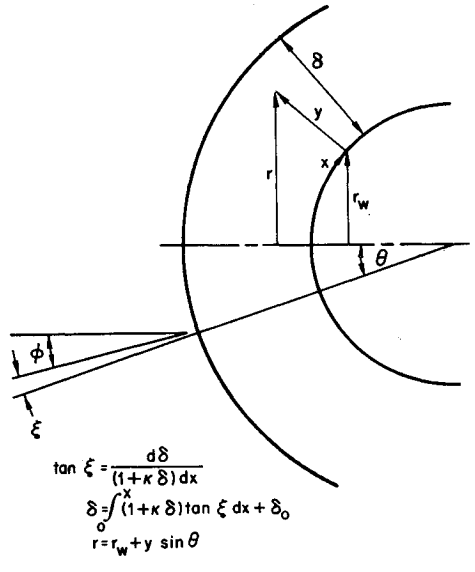

Fig. 3 Body-oriented coordinate system.

from which we obtain

$$\frac{dH}{d\eta} = -\frac{\cos\xi\beta_0\tilde{\delta}\alpha T^4}{\cos\phi(r_\delta/r_w)^\nu} \quad \text{at} \quad \eta = 1 \tag{27}$$

In the Appendix, we demonstrate that the use of Eq. (2) in the energy equation requires that the temperature and, hence, the static enthalpy approach zero at the stagnation point. Since no energy absorption processes are considered, the static enthalpy must then remain zero along the entire body streamline. Hence, we require

$$h = 0 \quad \text{at} \quad \eta = 0 \tag{28}$$

If we allow the static enthalpy to be zero along the body streamline, the density must become unbounded, since the pressure is finite. Under these conditions, the only wall velocity condition that is consistent with the x-momentum equation at the wall,

$$\rho u(du/dx) = dp/dx$$

where dp/dx is finite, is the requirement that the wall velocity be zero everywhere. Physically, this is consistent with the zero static energy at the stagnation point. For, if the static enthalpy, and hence the temperature, is zero, the fluid particle loses all its energy and cannot expand about the body.

Since a linear velocity profile is used (see the following subsection) with only a single boundary condition specified at the shock, the solution does not yield this zero velocity condition. However, the failure of this wall condition is not serious, since the zero velocity result is not realistic. Moreover, any real effect of a velocity decrease near the wall is limited to a relatively small portion of the shock layer, where its effect on the integral method is negligible.

3.4 Velocity and Enthalpy Profiles

An examination of tangential velocity profiles for adiabatic flows[6, 17] indicate that the profiles can be closely approximated by a straight line. In the present analysis, the radiation cooling effect can produce large density gradients that may significantly alter the profiles from the adiabatic case. However, in the transformed coordinate system, the effects of density gradients are greatly reduced. Therefore, it is felt that the velocity profile in η can adequately be represented by a linear profile¶:

$$u/u_\delta = a_0 + a_1\eta \tag{29}$$

where the boundary condition at the shock,

$$1 = a_0 + a_1 \tag{30}$$

is used to eliminate one of the coefficients in Eq. (29).

The total enthalpy profile will vary considerably, depending upon the amount of energy loss and the location about the body. For nearly adiabatic flows, the total enthalpy is essentially constant at the shock value, except for a narrow region near the body where large gradients exist. Two profiles have been selected to assess their ability to produce the expected total enthalpy profile for nearly adiabatic flows:

$$H/H_\delta = b_0 + b_1\eta + b_2\eta^2 + b_3\eta^3 \tag{I}$$

$$H/H_\delta = b_4'\eta^{1/4} + b_3'\eta^{1/3} + b_2'\eta^{1/2} + b_0 \tag{II}$$

The boundary conditions used to evaluate the coefficient are $H/H_\delta = 1$ at $\eta = 1$ and Eqs. (27) and (28). For the special case of an exact adiabatic flow, profile I was used, but with boundary-condition equation (28) deleted and the order of the profile reduced to a quadratic.

¶ It should be noted that a quadratic profile in η was investigated for a spherical body, using the velocity derivative at the shock to eliminate the additional coefficient. The resulting profile was essentially linear in η, although, for large values of x (body angle $\theta = 60°$), the wall velocity was too low.

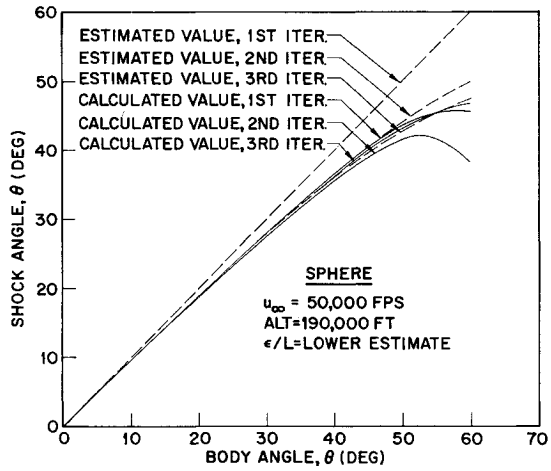

Fig. 4 Shock angle convergence.

4. Numerical Solution

Basically, the integral method requires that we determine shock-layer thickness and a given coefficient in both the velocity and total enthalpy profile so as to preserve conservation of mass, momentum, and energy in the large at each station about the body. In particular, at each point about the body, the integrals I_0, I_1, I_2 are calculated, and, together with the boundary conditions, these determine $\tilde{\delta}$ and the a_i's and b_i's. The η transformation, Eq. (15), is then inverted to obtain the physical shock thickness.

The determination of I_0, I_1, and I_2 is the essential part of the calculation. The integral I_0 is obtained directly from Eq. (13). However, I_1 and I_2 must be obtained by integration of the differential equations (18) and (21), which are statements of momentum and energy conservation between successive body stations. Both Eqs. (18) and (21) are first-order equations that can be solved as an initial value problem starting at the stagnation point. This condition, as pointed out by Maslen and Moeckel,[6] is a result of the effectively parabolic nature of the governing equations when terms of $O(\epsilon^2)$ are dropped from the y-momentum equation. Since the shock shape is specified, quantities like $\partial p/\partial x|_{y=\delta}$ that involve the shock curvature and, hence, terms containing $d^2\delta/dx^2$, are known. The combined effect of reducing the equations to $O(\epsilon)$ and specifying the shock shape permits a straightforward integration of the flow field.

An iteration procedure is used to determine the shock shape. The operational method used specifies the shock angle ϕ as a known function of the surface coordinate. Since the solution is more strongly dependent on the shock angle (i.e., on $d\delta/dx$) than on the standoff distance δ, the iteration scheme is based on a convergence of the shock angle. Figure 4 shows the results of this iteration procedure for flow past a sphere at a flight velocity of 50,000 fps, an altitude of 190,000 ft, and the lower emissivity estimate shown in Fig. 1. The estimated and calculated shock angles for each iteration are shown. For large body angles, the solution (i.e., the calculated ϕ values) is quite sensitive to the estimated shock angle. In order to avoid potentially unstable oscillations, the estimated shock shape for each iteration is adjusted to a physically meaningful value. This procedure also enhances the shock convergence. For the case shown in Fig. 4, the estimated and calculated shock angles for the third iteration agree within about 2%, which is judged sufficiently converged for most purposes.

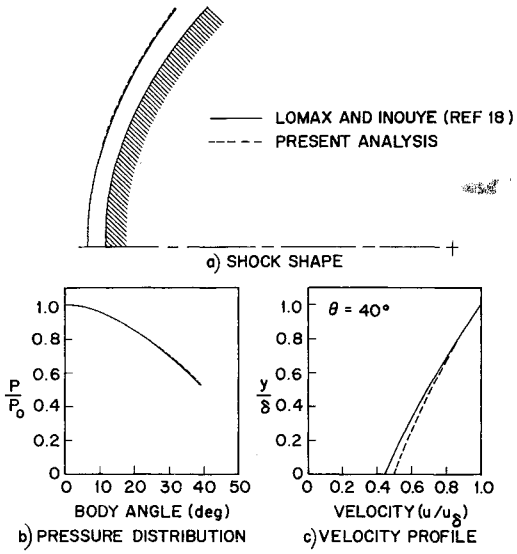

Fig. 5 Comparison of adiabatic solutions (u_∞ = 30,000 fps, altitude = 200,000 ft).

At the stagnation point, Eqs. (18) and (21) are singular since $u_\delta \to 0$ as $x \to 0$. By applying symmetry arguments to Eqs. (19) and (22), we find that dI_1/dx and dI_2/dx are zero at the stagnation point, and, of course, the shock wave is symmetric so that $d\delta/dx = 0$ at $x = 0$. These conditions together with a specified shock curvature at $x = 0$ are sufficient to define all stagnation-point values.

The exact thermodynamic properties of equilibrium air were used in obtaining the numerical results discussed in the next section. The correlations of Viegas and Howe[18] were used for temperatures below 15,000°K. Data calculated by Lockheed[19] were used to extend the NASA correlations to temperatures as high as 20,000°K and for pressures ranging from 0.01 to 10 atm.

5. Discussion of Results

Numerical solutions were obtained for the flow around a sphere and a 30° hemisphere-cone at flight velocities between 30,000 and 60,000 fps for flight altitudes of 190,000 and 200,000 ft. In Fig. 5, an adiabatic solution obtained by the present method is compared with the inverse numerical solution of Lomax and Inouye.[20] This adiabatic solution was obtained using a quadratic for the total enthalpy profile. No conditions were imposed to force the total enthalpy to remain constant. Instead, the total enthalpy profile was calculated as in the nonadiabatic case, since one purpose of obtaining an adiabatic solution was to determine how closely an exact adiabatic solution could be approximated using the integral method. The shock shape and surface pressure distribution are in excellent agreement with the exact numerical solution. The deviation is less than 2% over the portion of the body ($\theta \leq 40°$) for which data are available. The velocity profile at a body angle of 40° differs only slightly from the numerical solution of Lomax and Inouye. In general, the integral solution is in good agreement with the exact numerical solution. Hence, the integral method can be used to calculate the over-all flow-field characteristics and radiative heat transfer to the body for both adiabatic and nonadiabatic flows.

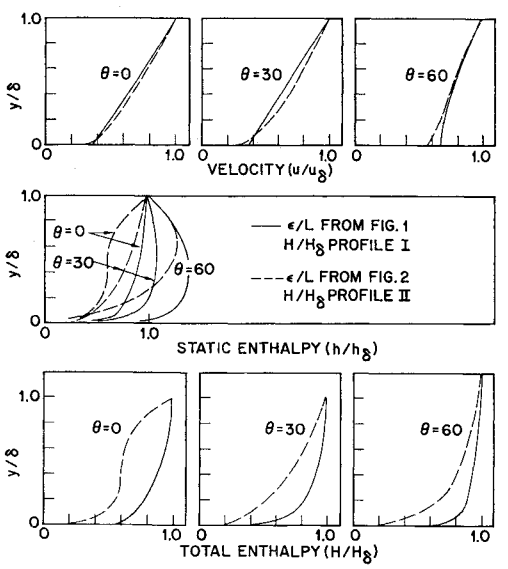

Fig. 6 Effect of energy loss on shock-layer profiles (u_∞ = 50,000 fps, altitude = 190,000 ft, R_b = 5 ft).

Solutions were obtained for the nonadiabatic flow past a sphere using the two enthalpy profiles shown in Sec. 3.4 for the case of u_∞ = 50,000 fps and an altitude of 190,000 ft. The lower emissivity estimate of Fig. 1 was used for these two cases so that only a small amount of energy loss occurred which yields a nearly adiabatic flow-field situation. Profile II, the inverse polynomial, produced the best results, in that the total enthalpy distribution through the shock layer was always less than the maximum value at the shock. This was not the case for the total enthalpy distribution obtained using profile I. The velocity distribution and shock shape were quite insensitive to the profile selection. When a case involving a substantial amount of energy loss from the shock layer was investigated, the enthalpy distribution in the stagnation region from profile II was unrealistic. However, profile I produced an enthalpy distribution in the stagnation region which closely approximated the distribution obtained from an analytic solution along the stagnation streamline.[21] These results indicate that profile II should be used when the energy losses are moderate ($\Gamma \sim 0.1$), whereas profile I should be used when the energy losses are substantial ($\Gamma \sim 1$).

The effect on the shock-layer flow field of increasing the amount of energy loss at fixed flight conditions was investigated by using the upper and lower emissivity estimates. For flight conditions of u_∞ = 50,000 fps and an altitude of 190,000 ft, the two emissivity estimates resulted in a difference of about an order of magnitude in degree of the energy loss. It was found that, for the high energy loss case ($\Gamma \sim 2.3$), shock standoff distance decreased by approximately a factor of 2 from the adiabatic value, demonstrating a strong coupling of the over-all flow field to the radiation field. The effect of the increased energy loss on the detailed structure of the flow field is shown in Fig. 6. Increasing the energy loss has little effect on the normalized velocity distribution

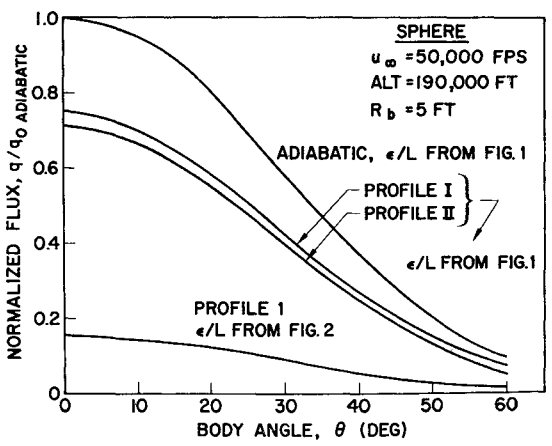

Fig. 7 Radiative heat-transfer distribution normalized to adiabatic stagnation-point value (u_∞ = 50,000 fps, altitude = 190,000 ft, R_b = 5 ft).

but significantly alters the total and static enthalpy distributions. Finally, it should be noted that the boundary condition on the static enthalpy at the wall $h(\eta = 0) = 0$, in effect, creates a radiation-cooled layer near the body surface. The extent of this region should depend on the degree of energy loss. That this is indeed the case is demonstrated by the total enthalpy distributions in Fig. 6.

The quantity of primary interest, namely, the radiative heating rate to the body surface, is shown in Fig. 7. These heating rates were obtained by assuming that, locally, the shock layer is approximated by an infinite plane slab with a nonuniform emission profile. The loss of energy by radiation results in substantial reductions in the radiative heating to the body. For the flight conditions shown in Fig. 7, the heating rates are reduced by 30 and 85% for the upper and lower emissivity data shown in Fig. 1. The reference quantity $(q_0)_{\text{adiabatic}}$ is the radiative heat rate obtained using the adiabatic shock detachment distance and the adiabatic shock-layer temperature. Approximately one-third to one-half of the reduction shown in Fig. 7 is due to the reduction in the shock detachment distance. The remainder is, of course, due to the increase in the local emission rate.

Note that the form of the total enthalpy, although having significant effects on the shock-layer profiles, has a small effect on the radiative heating. This can be explained on the basis that the radiative heating depends on an integration of the static enthalpy across the shock layer.

The radiative heat-transfer distribution about the body, normalized to the respective stagnation-point value, is presented in Fig. 8. These distributions have the rather surprising feature of being insensitive to the magnitude of the radiation cooling effect. The relative amount of energy loss in the shock layer (i.e., the difference of the total energy flux from the adiabatic shock-layer value) decreases about the body. This effect is observed in the "filling-out" of the total enthalpy profile (Fig. 6) at increasing distances about the body. The recovery of the total enthalpy profiles toward the adiabatic levels might be expected to yield a radiative heating distribution about the body which decays less rapidly than the adiabatic distribution. As seen in Fig. 8, this is not the case. Examination of the emission levels through the shock layer at various body locations discloses the reason why the radiative cooling effect persists about the body. For an adiabatic flow, the local emission increases toward the body so that a large portion of the heating comes from the hotter gas near the surface. However, for a nonadiabatic flow, the gas near the body has passed through the stagnation region and has lost a significant amount of energy. Therefore, for a nonadiabatic flow, the portion of the shock layer which would radiate the strongest is considerably cooled. This cooling explains the persistence of the reduced radiative heat transfer about the body.

The reduction in the stagnation-point radiative heat flux from the level obtained from an adiabatic (isothermal) shock layer is shown in Fig. 9. The results are plotted as a function of the radiation loss parameter Γ since, in the stagnation region and for the optically thin approximation, the effect of the radiant energy loss is determined principally by Γ. An examination of Fig. 9 shows that the data fall on a single curve when the Γ parameter is used. The integral method is in good agreement with Howe's stagnation-point solution. From Fig. 9 it can be seen that, even for Γ as low as 0.1, the nonadiabatic effects on the radiative heating are significant.

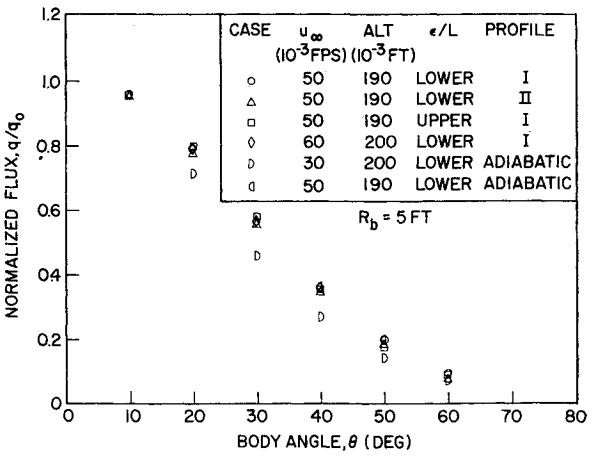

Fig. 8 Radiative heat-transfer distribution normalized to stagnation-point value.

Appendix

The velocity component normal to the body v is zero at the body surface. Hence, near the surface, the normal velocity can be expanded as the Taylor series

$$v = \sum_{i=1}^{n} a_i y^i \qquad \text{(A1)}$$

For y sufficiently small, but finite,

$$v = dy/dt = -ay \qquad \text{(A2)}$$

where a is a constant and t denotes time. Therefore, the time for a fluid particle to move from y_0 to y_1, where y_0 and y_1 are small but finite, is

$$t_1 = t_0 - \ln(y_1/y_0) \qquad \text{(A3)}$$

As the fluid particle approaches the body surface ($y_1 \to 0$), the residence time approaches infinity.

We consider, now, the behavior of a fluid particle from a Lagrangian viewpoint. The Lagrangian energy equation is

$$Dh/Dt_{\text{part}} = -4\pi\alpha B \qquad \text{(A4)}$$

Since the particle takes an infinite time to reach the wall, it must reach a steady-state condition at the wall:

$$Dh/Dt)_{\text{part}} \to 0 \quad \text{as} \quad y \to 0$$

However, the only way it can reach a steady-state condition is to have the emission term in the energy equation, the right-hand side of Eq. (A4), go to zero. This requires that the fluid particle have zero temperature (or enthalpy). Physically, the reason for this zero-temperature result is clear. Since a fluid particle takes an infinite time to reach the wall and since no absorption mechanisms have been included, the particle radiates away all of its energy.

It was pointed out in Sec. 3 that Eq. (A4) cannot be valid near the wall. If the gas becomes cold enough, even for a

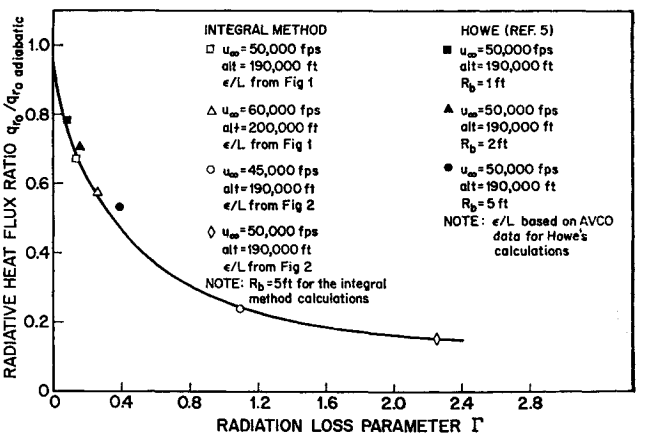

Fig. 9 Stagnation-point radiative heat flux reduction from adiabatic value.

very optically thin shock layer, the absorption at the wall emission must be included. Then Eq. (A4) becomes

$$Dh/Dt_{\text{part}} = -4\pi\alpha[B - (B_w/2)] \tag{A5}$$

and, as a steady-state condition is reached, we require

$$B \to B_w/2 \qquad \text{or} \qquad T \to (\tfrac{1}{2})^{1/4}T_w \tag{A6}$$

References

[1] Goulard, R., "The coupling of radiation and convection in detached shock layers," J. Quant. Spectry. Radiative Transfer **1**, 249–257 (December 1961).

[2] Bird, G. A., "The effect of thermal radiation on the inviscid hypersonic flow over a blunt body," J. Aerospace Sci. **27**, 713–714 (1960).

[3] Kennet, H., "Radiation-convection interaction around a sphere in hypersonic flow," ARS J. **32**, 1616–1617 (1962).

[4] Yoshikawa, K. K. and Chapman, D. R., "Radiative heat transfer and absorption behind a hypersonic normal shock wave," NASA TN D-1424 (September 1962).

[5] Howe, J. T. and Viegas, J. R., "Solutions of the ionized radiating shock layer, including readsorption and foreign species effects and stagnation region heat transfer," NASA TR R-159 (1963).

[6] Maslen, S. H. and Moeckel, W. E., "Inviscid hypersonic flow past blunt bodies," J. Aerospace Sci. **24**, 683–693 (1957).

[7] Meyerott, R. E., et al., "Absorption coefficients of air," Air Force Cambridge Research Labs., Geophys. Res. Paper 68 (1960).

[8] Armstrong, B. H., et al., "Radiative properties of temperature air," J. Quant. Spectry. Radiative Transfer **1**, 143–162 (November 1961).

[9] Stewart, J. C. and Pyatt, K. D., Jr., "Theoretical study of optical properties," Air Force Special Weapons Center TR-61-72, Vol. 1, General Atomic Div., General Dynamics (September 1961).

[10] Breene, R. G., et al., "Radiance of specie in high-temperature air," General Electric Co., MSD-R635D3 (June 1963).

[11] Rosseland, S., *Theoretical Astrophysics* (Clarendon Press, Oxford, England, 1936).

[12] Chandrasekhar, S., *An Introduction to the Study of Stellar Structure* (Dover Publications, Inc., New York, 1957), Chap. V.

[13] Unsöld, A., *Physik der Sternatmospharen* (Springer-Verlag, Berlin, 1955).

[14] Kourganoff, V., *Basic Methods in Transfer Problems* (Clarendon Press, Oxford, England, 1952).

[15] Goulard, R., "Fundamental equations of radiation gas dynamics," *The High Temperature Aspects of Hypersonic Flow*, edited by W. C. Nelson (Pergamon Press, New York, 1964), pp. 529–554.

[16] Viskanta, R., "Heat transfer in thermal radiation absorbing and scattering media," Argonne National Lab., ANL-6170 (May 1960).

[17] Hayes, W. D. and Probstein, R. F., *Hypersonic Flow Theory* (Academic Press, New York, 1959), Chap. 5.

[18] Viegas, J. R. and Howe, J. T., "Thermodynamic and transport property correlation formulas for equilibrium air from 1,000°K to 15,000°K," NASA TN D D-1429 (October 1962).

[19] "Study of heat shield requirements for manned Mars landing and return missions," Lockheed Missiles and Space Co. Quart. Progr. Rept. 804000 (March 17, 1964).

[20] Lomax, H. and Inouye, M., "Numerical analysis of flow properties about blunt bodies moving at supersonic speeds in an equilibrium gas," NASA Ames Research Center (in preparation).

[21] Chin, J. H. and Hearne, L. F., "Shock-layer radiation for sphere cones with radiative decay," Lockheed Missiles and Space Co. Rept. 5-13-64-4 (March 1964).